Analysis of a Multigrid Method for the Euler Equations of Gas Dynamics in Two Dimensions

Wim A. Mulder*
Department of Computer Science
Stanford University
Stanford, CA 94305-2140

The multigrid convergence factors of several relaxation schemes for the linearised upwind-differenced Euler equations are estimated by two-level local-mode analysis. Strong alignment, the flow being aligned with the grid, causes the failure of schemes that use only local data, such as Point-Jacobi, Red-Black, and Block-Jacobi relaxation. Damped collective symmetric Gauss-Seidel relaxation and an undamped version of Gauss-Seidel relaxation, with sweeps in all four directions, are both global relaxation schemes and can overcome this problem in the case of pure convection. However, they still fail for the full system of equations. This is confirmed by numerical experiments for the nonlinear Euler equations.

1. Introduction

The multigrid method is an efficient numerical technique for solving elliptic equations. It provides solutions within the truncation error for an amount of work proportional to the number of points or cells in the computational domain. Moreover, only one or a few multigrid iterations are required for regular elliptic problems. The theory for these kind of problems is well established. For details, the reader is referred to the textbook by Hackbusch [3].

Several attempts have been made to use the multigrid technique for the computation of steady solutions to hyperbolic partial differential equations, specifically the Euler equations that describe the flow of an inviscid compressible gas. Ni [15] was the first to obtain a significant acceleration with respect to a single-grid Lax-Wendroff scheme by using multiple grids. He employs explicit time-stepping as a relaxation scheme, which is hardly efficient. Jameson [6] uses central differencing, a four-stage Runge-Kutta time-stepping scheme, residual averaging, and enthalpy damping. Multigrid accelerates his scheme significantly. Jespersen [7] adopts a different approach, that is closely related to the standard multigrid technique for elliptic equations. Upwind differencing by means of flux-vector splitting [19] is used for the spatial discretisation and Symmetric Gauss-Seidel (SGS) for relaxation. Both the Correction Scheme (CS) and the Full Approximation Storage scheme (FAS) are studied. In the first, a global linearisation of the residual is computed, and the multigrid technique is applied to the linear system. In the latter, the nonlinear equations are used directly during the multigrid cycle.

In early 1983, without being aware of the work just mentioned, I implemented a multigrid method after reading a paper by Brandt [2], and found grid-independent convergence factors for a transonic test problem with a shock [11]. A flux-vector-splitting version by van Leer

This work has been supported by the Center for Large Scale Scientific Computing (CLaSSiC) Project at Stanford under the Office of Naval Research Contract N00014-82-K-0335.

* Present address: *Department of Mathematics, 405 Hilgard Avenue, University of California at Los Angeles, Los Angeles, CA 90024-1555.*

[22] is used for the upwind differencing of the isenthalpic Euler equations. This approximate Riemann-solver is continuously differentiable, a property shown to be desirable in [10]. Grid transfer is based on the finite-volume residual operator, resulting in Galerkin coarsening. Symmetric Gauss-Seidel is chosen as the relaxation scheme, based on earlier work in [23]. The CS scheme is used to solve the linear system arising from a Switched Evolution/Relaxation (SER) method. The latter can be viewed as a global Newton method. It is derived from a "backward Euler" implicit time-discretisation, with a "time-step" inverse proportional to some norm of the residual. Thus, if the solution is far away from the steady state, the residual is large, and a more or less time-accurate integration is carried out. Once the solution approaches the steady state, the scheme switches to Newton's method. The inclusion of the finite "time-step" is necessary in the case of a singular residual to avoid divergence. With this method and for the specific transonic test problem, grid-independent convergence factors are found both for a first-order- and second-order-accurate spatial discretisation. For the latter, a version of the Defect Correction Method [3:Eq.(14.3.1)] is used with a second-order-accurate residual and a linear system based on a first-order discretisation. Second-order accuracy is obtained by van Leer's technique [20,21]. The nonlinear generalisation of this method is sketched at the end of [11], but no experimental results are presented.

In hindsight, this method turns out to be very similar to Jespersen's. The main difference is the finite-volume approach leading to volume-averaging for restriction and zero-order interpolation for prolongation, rather than the nodal point approach of Jespersen that requires full weighting for restriction and bilinear interpolation for prolongation.

Following the work in [7] and [11], several authors have experimented with the multigrid method for the upwind-differenced Euler equations, using either the Correction or the FAS scheme. Hemker and Spekreijse [4] incorporate first-order upwind differencing, Galerkin coarsening, and nonlinear SGS relaxation in a FAS scheme. Osher's scheme [16] rather than van Leer's flux-vector splitting (FVS) is used for the upwind differencing. This scheme is continuously differentiable, just as FVS, but more accurate (at a higher cost). The higher accuracy allows for overspecification at the boundaries, in contrast to FVS where characteristic boundary conditions are required. Apart from this and the nonlinear implementation, the fundamental difference between their and my approach is the omission of the "time-step". This will cause their method to diverge in case of a locally singular residual, whereas the insertion of a "time-step" would at least guarantee stability. This issue will be discussed in more detail in §7. In spite of this, their method provides grid-independent convergence factors for a test problem similar to the one in [11]. Second-order-accurate results with Osher's scheme for the upwind differencing, van Leer's technique [20,21] for the second-order accuracy, and the Defect Correction technique for computing the solution, are presented in [5,9].

An application with strong shocks can be found in [12]. There, the relaxation scheme is symmetric line Gauss-Seidel, with the line relaxation in the periodic direction of the polar grid. Grid-independent convergence can not be observed, as the computations are restricted to relatively coarse grids. Three-dimensional computations with the FAS scheme and flux-vector splitting have been carried out by Anderson [1]. The relaxation scheme is Approximate Factorisation and the results suggest grid-independent convergence factors. An extension of the work in [11] to the Navier-Stokes equations is reported in [17]. Here grid-independent convergence factors are obtained as well. A later example is [18].

In summary, there is experimental evidence that the combination of upwind differencing and Symmetric Gauss-Seidel or another type of relaxation scheme is capable of producing grid-independent convergence factors. It should be stressed, however, that none of the studies mentioned above are extended to very fine grids. Also, there are practically no theoretical results to support the claims of grid-independent convergence rates.

An attempt to predict multigrid convergence factors for purely convective equations can be found in [13]. There the one-dimensional scalar inviscid Burgers' equation is considered. Of course, it does not make much sense to use the multigrid method for one-dimensional problems. However, some interesting results were found. First of all, it turns out that optimising the smoothing rate of the relaxation scheme does not necessarily imply a good multigrid convergence rate. Secondly, the discrete equations become singular at the shock. This is is consistent with the differential equations. With a special treatment of shocks after prolongation, a good agreement between experimental and predicted convergence factors is obtained. Otherwise, convergence is slower than predicted, but still acceptable for some relaxation schemes. Damped Point-Jacobi relaxation appears to be the most attractive scheme.

In this paper we extend the two-level local-mode analysis to two dimensions. Only the linearised Euler equations with constant coefficients and periodic boundaries are considered (§2). Nonlinear effects are not addressed in this paper. The upwind discretisation is described in §3. The coarse-grid correction operator is evaluated in §4. It describes the result of restriction to a coarser grid, solving the coarse-grid equations exactly, and prolongating the coarse-grid correction back to the fine grid. Several relaxation schemes are considered in §5. As in the one-dimensional case [13], we would prefer to have a scheme that uses only local information, as these schemes are easily vectorised and are more convenient to use on parallel architectures. Also, their flexibility makes them better suited for applications with adaptive grid-refinement. Investigated are: Point-Jacobi relaxation, a Multi-Stage scheme, Red-Black or checkerboard relaxation, and Block-Jacobi. As global relaxation schemes, Gauss-Seidel relaxation and its symmetric variants are considered.

Multigrid convergence factors are estimated in §6. The schemes just mentioned fail because of strong alignment, the flow being aligned with the grid, which is a well-known problem for elliptic equations with strongly anisotropic coefficients [2,3]. For pure convection, this problem can be overcome by damped symmetric Gauss-Seidel (SGS) or by a version of Gauss-Seidel with sweeps in all four directions (S^2GS). However, these global relaxation scheme still fail for the full system of Euler equations.

Because the Fourier modes are not the proper eigenfunctions of the GS relaxation operator, some numerical experiments on the nonlinear Euler equations are carried out (§7). The failure of S^2GS and damped SGS is confirmed.

The main results are summarised in §8. Some alternatives for obtaining uniformly good convergence rates are discussed.

2. Model equations

The two-level local-mode analysis [2] will be carried out on a linearised form of the Euler equations. These equations are given below.

The Euler equations in conservation form, describing the dynamics of an inviscid compressible gas, are

$$\frac{\partial w'}{\partial t} + \frac{\partial f}{\partial x} + \frac{\partial g}{\partial y} = 0. \tag{2.1a}$$

The vector of states w' and the fluxes f and g are

$$w' = \begin{pmatrix} \rho \\ \rho u \\ \rho v \\ \rho E \end{pmatrix}, \quad f = \begin{pmatrix} \rho u \\ \rho u^2 + p \\ \rho uv \\ \rho uH \end{pmatrix}, \quad g = \begin{pmatrix} \rho v \\ \rho uv \\ \rho v^2 + p \\ \rho vH \end{pmatrix}. \tag{2.1b}$$

Here ρ is the density of the gas, and u and v are the x- and y-component of the velocity, respectively. The energy E, total enthalpy H, pressure p, and sound speed c are related by

$$E = \frac{1}{(\gamma-1)}\frac{p}{\rho} + \tfrac{1}{2}(u^2+v^2), \quad H = E + p/\rho, \quad c^2 = \gamma p/\rho. \tag{2.2}$$

Linearising (2.1) and applying a similarity transform based on

$$P = \rho \begin{pmatrix} 0 & 0 & 1/c & -1/\gamma \\ 1 & 0 & u/c & -u/\gamma \\ 0 & 1 & v/c & -v/\gamma \\ u & v & H/c & -\frac{1}{2}(u^2+v^2)/\gamma \end{pmatrix}, \tag{2.3}$$

we obtain

$$\frac{\partial w}{\partial t} + A\frac{\partial w}{\partial x} + B\frac{\partial w}{\partial y} = 0, \tag{2.4a}$$

with the symmetric matrices

$$A = P^{-1}\frac{\partial f}{\partial w'}P = \begin{pmatrix} u & 0 & c & 0 \\ 0 & u & 0 & 0 \\ c & 0 & u & 0 \\ 0 & 0 & 0 & u \end{pmatrix}, \quad B = P^{-1}\frac{\partial g}{\partial w'}P = \begin{pmatrix} v & 0 & 0 & 0 \\ 0 & v & c & 0 \\ 0 & c & v & 0 \\ 0 & 0 & 0 & v \end{pmatrix}. \tag{2.4b}$$

The vector w obeys

$$\delta w = P^{-1}\delta w' = \begin{pmatrix} \delta u \\ \delta v \\ \frac{1}{\rho c}\delta p \\ \delta S \end{pmatrix}, \tag{2.5}$$

where the specific entropy $S = \log(p/\rho^\gamma)$. The fourth equation of the system (2.4) describes the convection of the entropy along streamlines. The remaining 3×3 system represents the combination of convection and sound waves. In the isentropic case, the fourth equation can be dropped and the third component of w (2.5) becomes $2c/(\gamma-1)$.

The matrix $\kappa_1 A + \kappa_2 B$, with $\kappa_1^2 + \kappa_2^2 = 1$, can be diagonalised:

$$\kappa_1 A + \kappa_2 B = Q\Lambda Q^{-1}, \tag{2.6a}$$

where

$$Q = \begin{pmatrix} \kappa_1 & \kappa_2 & 0 & \kappa_1 \\ \kappa_2 & -\kappa_1 & 0 & \kappa_2 \\ -1 & 0 & 0 & 1 \\ 0 & 0 & 1 & 0 \end{pmatrix}, \tag{2.6b}$$

and

$$\Lambda = \begin{pmatrix} \kappa_1 u + \kappa_2 v - c & & & \\ & \kappa_1 u + \kappa_2 v & & \\ & & \kappa_1 u + \kappa_2 v & \\ & & & \kappa_1 u + \kappa_2 v + c \end{pmatrix}. \tag{2.6c}$$

In the following sections we will consider the linear system (2.4) with constant coefficients and periodic boundary conditions.

3. Discretisation

The spatial discretisation of (2.4) is obtained by upwind differencing. The upwind differencing is carried out separately for the x- and y-direction. For each characteristic variable, the upwind direction is determined from the eigenvalues of A or B. The resulting residual operator is given below. The singularities of its symbol are listed as well.

For the upwind differencing in the x-direction, the matrix A is diagonalised by

$$A = Q_1\Lambda_1 Q_1^{-1}, \quad Q_1 = Q(\kappa_1 = 1, \kappa_2 = 0), \quad \Lambda_1 = \Lambda(\kappa_1 = 1, \kappa_2 = 0), \tag{3.1a}$$

where Λ_1 is the diagonal matrix. For the y-direction we have

$$B = Q_2\Lambda_2 Q_2^{-1}, \quad Q_2 = Q(\kappa_1 = 0, \kappa_2 = 1), \quad \Lambda_2 = \Lambda(\kappa_1 = 0, \kappa_2 = 1). \tag{3.1b}$$

We define Λ^+ and Λ^- as the matrices that contain the positive and negative elements of Λ, respectively. This implies

$$\Lambda^+ + \Lambda^- = \Lambda, \quad \Lambda^+ - \Lambda^- = |\Lambda|. \tag{3.2}$$

Now define

$$A^\pm \equiv Q_1\Lambda_1^\pm Q_1^{-1}, \quad B^\pm \equiv Q_2\Lambda_2^\pm Q_2^{-1}. \tag{3.3}$$

It follows that

$$\begin{aligned} A &= A^+ + A^-, \quad |A| \equiv Q_1|\Lambda_1|Q_1^{-1} = A^+ - A^-; \\ B &= B^+ + B^-, \quad |B| \equiv Q_2|\Lambda_2|Q_2^{-1} = B^+ - B^-. \end{aligned} \tag{3.4}$$

The upwind-differenced linear residual operator

$$L^h = \frac{1}{h_x}[A^+(1-T_x^{-1}) + A^-(T_x - 1)] + \frac{1}{h_y}[B^+(1-T_y^{-1}) + B^-(T_y - 1)]. \tag{3.5}$$

The shift operators T_x and T_y are defined by $T_x w_{k_1,k_2} \equiv w_{k_1+1,k_2}$, $T_y w_{k_1,k_2} \equiv w_{k_1,k_2+1}$. Only a uniform grid will be considered ($h_x = h_y = h$).

The steady state problem is written in terms of the error $v^h \equiv \overline{w}^h - w^h$, where $\overline{w}^h$ is the stationary solution. The Fourier transform of v^h for a $N_1 \times N_2$ grid is

$$\hat{v}^h_{l_1,l_2} = \frac{1}{N_1 N_2}\sum_{k_1=0}^{N_1-1}\sum_{k_2=0}^{N_2-1} v^h_{k_1,k_2}\exp\left[-i\left(k_1\theta_x + k_2\theta_y\right)\right], \tag{3.6a}$$

where the frequencies

$$\theta_x = 2\pi\frac{l_1}{N_1}, \quad \theta_y = 2\pi\frac{l_2}{N_2}, \quad l_1 = -(\tfrac{1}{2}N_1 - 1), \ldots, \tfrac{1}{2}N_1, \quad l_2 = -(\tfrac{1}{2}N_2 - 1), \ldots, \tfrac{1}{2}N_2. \tag{3.6b}$$

The symbols of the shift-operators T_x and T_y are

$$\hat{T}_x = \exp(i\theta_x), \quad \hat{T}_y = \exp(i\theta_y), \quad -\pi < \theta_x \le \pi, \quad -\pi < \theta_y \le \pi. \tag{3.7}$$

Lemma 3.1. *The linearised residual operator $\hat{L}^h$ is singular only in each of the following cases:*

$$\begin{aligned} &(i) \quad \hat{T}_x = 1, \hat{T}_y = 1 \\ &(ii) \quad \hat{T}_x \neq 1, \hat{T}_y = 1: \ u = -c \text{ or } u = 0 \text{ or } u = c; \\ &(iii) \quad \hat{T}_x = 1, \hat{T}_y \neq 1: \ v = -c \text{ or } v = 0 \text{ or } v = c; \\ &(iv) \quad \hat{T}_x \neq 1, \hat{T}_y \neq 1: \ u = v = 0. \end{aligned} \tag{3.8}$$

Proof. In the first case, the lincarised residual operator $\hat{L}^h = 0$. In the second case we have

$$h\hat{L}^h = A^+(1 - \hat{T}_x^{-1}) + A^-(\hat{T}_x - 1), \tag{3.9}$$

This expression can be diagonalised by Q_1, yielding eigenvalues

$$|\lambda_{1\,l}|(1 - \cos\theta_x) + i\lambda_{1\,l}\sin\theta_x, \quad l = 1, \ldots, 4. \tag{3.10}$$

This expression only vanishes if $\lambda_{1\,l} = 0$, i.e., if one of the eigenvalues of A vanishes. The third case is proven in the same way. For case *(iv)* we write the linearised residual operator as

$$h\hat{L}^h = |A|(1 - \cos\theta_x) + |B|(1 - \cos\theta_y) + i(A\sin\theta_x + B\sin\theta_y). \tag{3.11}$$

A necessary condition for $\hat{L}^h$ to be singular is that its real part have a zero eigenvalue. The matrix

$$\mu_1|A| + \mu_2|B|, \quad \mu_1 > 0, \ \mu_2 > 0. \tag{3.12}$$

is singular only for $u = v = 0$. It is easily seen that $\hat{L}^h$ is also singular for this choice. □

4. Coarse-grid correction operator

An estimate of the multigrid convergence rate for a given residual operator can be obtained by considering 2 grids, a fine and a coarse. The multigrid convergence factor is determined by the combination of relaxation on the fine grid and corrections to the solution from the coarse grid. Here we will describe the latter. Attention is given to the singularities of the coarse-grid equations, and the stability of the coarse-grid correction operator.

The coarse-grid correction (CGC) operator K describes the effect of the following sequence of operations. First the fine-grid residual $L^h v^h$ is restricted to the coarser grid. The restriction operator is written as I_h^H, where $H = 2h$. Next it is assumed that the steady-state problem on the coarser grid is solved exactly. Finally, the coarse-grid correction is prolongated back to the fine grid. The prolongation operator is denoted by I_H^h. The CGC operator is given by

$$K = I - I_H^h \left(L^H\right)^{-1} I_h^H L^h. \tag{4.1}$$

Here I is the identity operator. Volume-averaging is adopted for the restriction operator, and zero-order interpolation is used for prolongation [11].

The restriction operator introduces a coupling between the frequencies on the fine grid: θ_x is coupled with $\theta_x + \pi$, and θ_y with $\theta_y + \pi$. For brevity we define

$$\begin{aligned} \hat{v}^h_{++} &\equiv \hat{v}^h(\ \hat{T}_x,\ \hat{T}_y) = \hat{v}^h(\theta_x\ \ \ ,\theta_y\ \ \ ), \\ \hat{v}^h_{-+} &\equiv \hat{v}^h(-\hat{T}_x,\ \hat{T}_y) = \hat{v}^h(\theta_x + \pi, \theta_y\ \ \ ), \\ \hat{v}^h_{+-} &\equiv \hat{v}^h(\ \hat{T}_x, -\hat{T}_y) = \hat{v}^h(\theta_x\ \ \ ,\theta_y + \pi), \\ \hat{v}^h_{--} &\equiv \hat{v}^h(-\hat{T}_x, -\hat{T}_y) = \hat{v}^h(\theta_x + \pi, \theta_y + \pi). \end{aligned} \tag{4.2a}$$

Here $\hat{v}^h$ denotes the Fourier transform of the error v^h. Furthermore,

$$\hat{V}^h \equiv \begin{pmatrix} \hat{v}^h_{++} \\ \hat{v}^h_{-+} \\ \hat{v}^h_{+-} \\ \hat{v}^h_{--} \end{pmatrix}, \tag{4.2b}$$

a vector with 4×4 elements.

Let the fine grid be numbered by indices (k_1, k_2), with k_1 running from 0 to $N_1 - 1$, and k_2 from 0 to $N_2 - 1$. On the coarse grid we can use the same indices, but now $k_1 = 0, \ldots, \frac{1}{2}N_1 - 1$ and $k_2 = 0, \ldots, \frac{1}{2}N_2 - 1$. The restriction operator coarsens an arbitrary discrete variable a^h to $a^H = I_h^H a^h$ according to

$$a^H_{k_1,k_2} = \tfrac{1}{4}(a^h_{2k_1,2k_2} + a^h_{2k_1+1,2k_2} + a^h_{2k_1,2k_2+1} + a^h_{2k_1+1,2k_2+1}). \tag{4.3}$$

The Fourier transform of the restricted fine-grid residual in terms of waves on the fine grid is given by

$$\hat{I}_h^H \hat{L}^h = \begin{pmatrix} \hat{R}_{++} & \hat{R}_{-+} & \hat{R}_{+-} & \hat{R}_{--} \end{pmatrix} \begin{pmatrix} \hat{L}^h_{++} & & & \\ & \hat{L}^h_{-+} & & \\ & & \hat{L}^h_{+-} & \\ & & & \hat{L}^h_{--} \end{pmatrix}, \tag{4.4a}$$

where

$$\hat{R}_{++} = \hat{R}(\hat{T}_x, \hat{T}_y) = \tfrac{1}{4}(1 + \hat{T}_x)(1 + \hat{T}_y). \tag{4.4b}$$

Here the convention (4.2a) is used. The coarse-grid residual operator

$$\hat{L}^H = \tfrac{1}{2h}[A^+(1 - \hat{T}_x^{-2}) + A^-(\hat{T}_x^2 - 1) + B^+(1 - \hat{T}_y^{-2}) + B^-(\hat{T}_y^2 - 1)], \tag{4.5}$$

which can be obtained by Galerkin coarsening $(\hat{I}_h^H \hat{L}^h \hat{I}_H^h)$ or by direct evaluation. We ignore the singular behaviour of $\hat{L}^H$ for a moment. The coarse-grid correction operator

$$\hat{K} = I - \begin{pmatrix} \hat{P}_{++} \\ \hat{P}_{-+} \\ \hat{P}_{+-} \\ \hat{P}_{--} \end{pmatrix} \begin{pmatrix} \hat{Z}_{++} & \hat{Z}_{-+} & \hat{Z}_{+-} & \hat{Z}_{--} \end{pmatrix}, \tag{4.6a}$$

where

$$\hat{P}_{++} = \tfrac{1}{4}(1+\hat{T}_x^{-1})(1+\hat{T}_y^{-1}), \quad \hat{Z}_{\pm\pm} \equiv \left(\hat{L}^H\right)^{-1}\hat{R}_{\pm\pm}\hat{L}_{\pm\pm}. \tag{4.6b}$$

Note that the prolongation operator is the conjugate transpose of the restriction operator in Fourier space. The identity matrix I in (4.6a) has a size 16×16. The CGC operator should be applied to the vector $\hat{V}^h$. Because $\hat{K}$ operates on 4 waves simultaneously, we only have to consider half the frequency domain in each direction, i.e., $0 \le \theta_x < \pi$ and $0 \le \theta_y < \pi$.

If $\hat{L}^H$ is singular, its pseudo-inverse should be used. To justify this, we assert the following.

Lemma 4.1. *Let the coarse-grid residual $\hat{L}^H$ and the restriction $\hat{R}_{\pm\pm}$ of the fine-grid residual be of the form given above. Then the linear system*

$$\hat{L}^H\hat{Z}_{\pm\pm} = \hat{R}_{\pm\pm}\hat{L}_{\pm\pm} = \tfrac{1}{4}(1\pm\hat{T}_x)(1\pm\hat{T}_y)\hat{L}^h_{\pm\pm} \tag{4.7}$$

is consistent.

Proof. If $\hat{L}^H$ is not singular, then this is trivial. The singularities of $\hat{L}^H$ correspond to those of $\hat{L}^h$, if $(\hat{T}_x, \hat{T}_y)$ in the latter is replaced by $(\hat{T}_x^2, \hat{T}_y^2)$. The singularities in $\hat{L}^h$ are listed in Lemma 3.1. In the first case, $\hat{T}_x^2 = \hat{T}_y^2 = 1$ implies $\hat{R}_{\pm\pm}\hat{L}_{\pm\pm} = 0$, so the linear system (4.7) is consistent. In the second case, $\hat{R}_{\pm-}\hat{L}_{\pm-} = 0$. What remains reduces to

$$(\hat{T}_x^{-2}A^+ + A^-)\hat{Z}_{\pm+} = (\pm\hat{T}_x^{-1}A^+ + A^-). \tag{4.8a}$$

Diagonalisation by Q_1 yields

$$(\hat{T}_x^{-2}\lambda_{1l}^+ + \lambda_{1l}^-)(Q_1^{-1}\hat{Z}_{\pm+}Q_1)_l = (\pm\hat{T}_x^{-1}\lambda_{1l}^+ + \lambda_{1l}^-), \quad l = 1,\ldots,4. \tag{4.8b}$$

This is singular only if $\lambda_{1l} = 0$, for which (4.8b) is consistent. Case *(iii)* is proven in a similar way.

In case *(iv)* we have to consider $u = v = 0$. Then the fourth row and fourth column of the left-hand and right-hand side of (4.7) have zeroes, implying consistency. The remaining 3×3 matrix on the left-hand side has a determinant

$$(c/2h)^3(1-\hat{T}_x^2)(1-\hat{T}_x^{-2})(1-\hat{T}_y^2)(1-\hat{T}_y^{-2}) \neq 0, \tag{4.9}$$

and is therefore non-singular. □

Lemma 4.2. *If m is the rank of $\hat{L}^H$, then the coarse-grid correction operator has m zero eigenvalues, and $16-m$ eigenvalues equal to 1.*

Proof. Let the matrix

$$Q_K = \begin{pmatrix} P_{++} & 0 & 0 & 0 \\ P_{-+} & 1 & 0 & 0 \\ P_{+-} & 0 & 1 & 0 \\ P_{--} & 0 & 0 & 1 \end{pmatrix}, \quad Q_K^{-1} = \begin{pmatrix} 1/P_{++} & 0 & 0 & 0 \\ -P_{-+}/P_{++} & 1 & 0 & 0 \\ -P_{+-}/P_{++} & 0 & 1 & 0 \\ -P_{--}/P_{++} & 0 & 0 & 1 \end{pmatrix}. \tag{4.10}$$

Note that Q_K is a regular matrix for $0 \le \theta_x < \pi$ and $0 \le \theta_y < \pi$. Because Q_K does not contain $A^\pm$ or $B^\pm$, we can carry out a similarity transform as if $\hat{K}$ was just a 4×4 matrix with scalar entries rather than 4×4 blocks. The result is

$$\hat{K}' = Q_K^{-1}\hat{K}Q_K = \begin{pmatrix} 1-\left(\hat{L}^H\right)^{-1}\hat{L}^H & -\hat{Z}_{-+} & -\hat{Z}_{+-} & -\hat{Z}_{--} \\ 0 & 1 & 0 & 0 \\ 0 & 0 & 1 & 0 \\ 0 & 0 & 0 & 1 \end{pmatrix}. \tag{4.11}$$

For a regular $\hat{L}^H$, we obviously have 12 eigenvalues equal to 1, and 4 equal to 0. For a singular $\hat{L}^H$ of rank $m < 4$, the use of the pseudo-inverse causes $[1-(\hat{L}^H)^\dagger\hat{L}^H]$ to have m eigenvalues 0 and $4-m$ eigenvalues 1. □

5. Relaxation

In this section several relaxation schemes are considered. They are presented in a form that is compatible with the coarse-grid correction operator. A relaxation scheme is constructed by replacing the residual operator L^h by an operator $\tilde{L}^h$ that can be easily inverted. Then the error is updated according to

$$\tilde{L}^h(\tilde{v}^h - v^h) = -L^h v^h. \tag{5.1}$$

In the following, we set $h = h_x = h_y = 1$. Some useful definitions are:

$$\begin{aligned} L^h &= M_0 - M_1 - M_2, & M_1 &\equiv A^+T_x^{-1} + B^+T_y^{-1}, \\ M_0 &\equiv |A| + |B|, & M_2 &\equiv -A^-T_x - B^-T_y. \end{aligned} \tag{5.2}$$

The general form of a relaxation operator, acting on $\hat{V}^h$ (4.2b), is

$$\hat{S} = \begin{pmatrix} \hat{G}_{1,++} & \hat{G}_{2,++} & \hat{G}_{3,++} & \hat{G}_{4,++} \\ \hat{G}_{2,-+} & \hat{G}_{1,-+} & \hat{G}_{4,-+} & \hat{G}_{3,-+} \\ \hat{G}_{3,+-} & \hat{G}_{4,+-} & \hat{G}_{1,+-} & \hat{G}_{2,+-} \\ \hat{G}_{4,--} & \hat{G}_{3,--} & \hat{G}_{2,--} & \hat{G}_{1,--} \end{pmatrix}. \tag{5.3}$$

We start with schemes for which $\hat{G}_2 = \hat{G}_3 = \hat{G}_4 = 0$, i.e., there is no coupling of frequencies.

The simplest relaxation scheme is Point-Jacobi. It updates the error according to

$$\tilde{v}^h = \left[1 - \beta M_0^{-1}L^h\right]v^h, \tag{5.4a}$$

implying

$$\hat{G}_{++}^{PJ} = 1 - \beta M_0^{-1}\hat{L}^h_{++}, \tag{5.4b}$$

The other $\hat{G}_{\pm\pm}^{PJ}$ follow by the convention (4.2a). The parameter β describes the amount of under- or overrelaxation. Standard Point-Jacobi is obtained for $\beta = 1$. The scheme is stable for $0 \le \beta \le 1$, so overrelaxation is excluded. The matrix M_0 is positive semi-definite. It becomes singular for $u = v = 0$. In that case the pseudo-inverse should be taken for M_0^{-1}.

Note that this is only done for the purpose of analysis. A different approach is adopted for the numerical experiments in §7.

A Multi-Stage method with two stages is obtained by first performing a PJ-step to an intermediate level, and then using the residual at the intermediate level to make the full step from the old to the new level:

$$\begin{aligned} v^{h*} &= v^h - \beta_1 M_0^{-1} L^h v^h, \\ \tilde{v}^h &= v^h - \beta_2 M_0^{-1} L^h v^{h*}. \end{aligned} \tag{5.5a}$$

This implies

$$G^{MS} = 1 - \beta_2 M_0^{-1} L^h \left(1 - \beta_1 M_0^{-1} L^h\right). \tag{5.5b}$$

Now we have two parameters β_1 and β_2.

We proceed with the schemes that introduce a coupling between frequencies. Red-Black or checkerboard relaxation is a scheme that first performs a PJ-step on the cells with indices $(2k_1, 2k_2)$ and $(2k_1+1, 2k_2+1)$. Then new residuals are computed, and the cells with indices $(2k_1+1, 2k_2)$ and $(2k_1, 2k_2+1)$ are updated by a PJ-step. This variant will be denoted by RB1. The variant that relaxes in the opposite order will be called RB2. For RB1:

$$\begin{aligned} &\hat{G}^{RB1}_{1,++} = 1 - \beta M_0^{-1} \hat{L}^h_{++} - \hat{G}^{RB1}_{4,--}, \\ &\hat{G}^{RB1}_{2,\pm\pm} = \hat{G}^{RB1}_{3,\pm\pm} = 0, \quad \hat{G}^{RB1}_{4,++} = \tfrac{1}{2}\beta^2 M_0^{-1}(\hat{M}_{1,--} + \hat{M}_{2,--}) M_0^{-1} \hat{L}^h_{--}. \end{aligned} \tag{5.6}$$

For RB2 we have

$$\hat{G}^{RB2}_{1,\pm\pm} = \hat{G}^{RB1}_{1,\pm\pm}, \quad \hat{G}^{RB2}_{2,\pm\pm} = \hat{G}^{RB2}_{3,\pm\pm} = 0, \quad \hat{G}^{RB2}_{4,\pm\pm} = -\hat{G}^{RB1}_{4,\pm\pm}. \tag{5.7}$$

The distinction between RB1 and RB2 becomes important if the relaxation scheme is used in combination with the CGC operator (as in [13]).

Another relaxation scheme is obtained if the 4 cells contained within one coarse-grid cell are relaxed simultaneously, ignoring the contributions from outside the 4 cells. This method is called Block-Jacobi. In physical space we have

$$\begin{pmatrix} M_0 & A^- & B^- & 0 \\ -A^+ & M_0 & 0 & B^- \\ -B^+ & 0 & M_0 & A^- \\ 0 & -B^+ & -A^+ & M_0 \end{pmatrix} \left(\tilde{V}^h - V^h\right) = -\beta \begin{pmatrix} L^h & & & \\ & L^h & & \\ & & L^h & \\ & & & L^h \end{pmatrix} V^h, \tag{5.8a}$$

where

$$V^h \equiv \begin{pmatrix} v_{2k_1,\,2k_2} \\ v_{2k_1+1,2k_2} \\ v_{2k_1,\,2k_2+1} \\ v_{2k_1+1,2k_2+1} \end{pmatrix}. \tag{5.8b}$$

In Fourier space

$$\hat{S}^{BJ} = I - \beta \hat{H}^{-1} \begin{pmatrix} \hat{L}^h_{++} & & & \\ & \hat{L}^h_{-+} & & \\ & & \hat{L}^h_{+-} & \\ & & & \hat{L}^h_{--} \end{pmatrix}. \tag{5.9a}$$

Here $\hat{H}$ has the same structure as $\hat{S}$ in (5.3), with elements

$$\begin{aligned} &\hat{H}_{1,++} = M_0 - \tfrac{1}{2}(\hat{M}_1 + \hat{M}_2), \qquad \hat{H}_{2,++} = -\tfrac{1}{2}(A^+ \hat{T}_x^{-1} + A^- \hat{T}_x), \\ &\hat{H}_{3,++} = -\tfrac{1}{2}(B^+ \hat{T}_y^{-1} + B^- \hat{T}_y), \quad \hat{H}_{4,++} = 0. \end{aligned} \tag{5.9b}$$

Finally, consider Gauss-Seidel relaxation. This is a global relaxation method, in contrast to the schemes mentioned above. In two dimensions there are four sweep directions. The relaxation operators for each direction are

$$\begin{aligned} &\textit{north-east}\ (\nearrow) \quad \hat{G}^{GS1} = 1 - \beta \left[\hat{L}^h - A^- \hat{T}_x \ - B^- \hat{T}_y \ \right]^{-1} \hat{L}^h, \\ &\textit{south-west}\ (\swarrow) \quad \hat{G}^{GS2} = 1 - \beta \left[\hat{L}^h + A^+ \hat{T}_x^{-1} + B^+ \hat{T}_y^{-1}\right]^{-1} \hat{L}^h, \\ &\textit{south-east}\ (\searrow) \quad \hat{G}^{GS3} = 1 - \beta \left[\hat{L}^h - A^- \hat{T}_x \ + B^+ \hat{T}_y^{-1}\right]^{-1} \hat{L}^h, \\ &\textit{north-west}\ (\nwarrow) \quad \hat{G}^{GS4} = 1 - \beta \left[\hat{L}^h + A^+ \hat{T}_x^{-1} - B^- \hat{T}_y \ \right]^{-1} \hat{L}^h. \end{aligned} \tag{5.10}$$

Here pseudo-inverses should be used if necessary. There are two variants for Symmetric Gauss-Seidel (SGS), namely $\hat{G}_2\hat{G}_1$ and $\hat{G}_4\hat{G}_3$. The variant that sweeps in all four directions will be denoted by S^{2}GS:

$$\hat{G}^{S2GS} \equiv \hat{G}_4\hat{G}_3\hat{G}_2\hat{G}_1. \tag{5.11}$$

It should be noted that this is not the correct way to carry out the analysis. The reason is the well-known fact that

$$\exp\left[2\pi i \left(k_1\theta_x + k_2\theta_y\right)\right], \tag{5.12}$$

is not an eigenfunction of the relaxation operator. Therefore, the Fourier analysis is not valid, although reasonable estimates may still be obtained for all but the longer waves.

6. Multigrid convergence factors

The multigrid convergence factor, also known as the asymptotic convergence rate, is given by

$$\overline{\lambda} \equiv \max_{\theta_x,\theta_y} \lambda(\theta_x,\theta_y), \quad \lambda(\theta_x,\theta_y) = \rho\left(\hat{S}^{\nu_2}\hat{K}\hat{S}^{\nu_1}\right). \tag{6.1}$$

The maximum is taken over the entire spectrum. The spectral radius is denoted by $\rho(\cdot)$ The operator describes ν_1 pre-relaxation sweeps on the finest grid, restriction to the next coarser grid, exact solution of the coarse-grid equations, prolongation of the coarse-grid correction to the finest grid, and, finally, ν_2 post-relaxation sweeps. In this section we will only consider the choice $\nu_1 = 1$, $\nu_2 = 0$.

For a singular residual operator, $\overline{\lambda}$ can become 1 for waves that are not seen by the operator, hence are not damped. In that case one better considers the multigrid convergence factor of the residual

$$\overline{\lambda}_r \equiv \max_{\theta_x,\theta_y} \lambda_r(\theta_x,\theta_y), \quad \lambda_r(\theta_x,\theta_y) \equiv \rho\left(\hat{L}^h\hat{S}^{\nu_2}\hat{K}\hat{S}^{\nu_1}(\hat{L}^h)^\dagger\right). \tag{6.2}$$

This quantity can be observed in numerical experiments (cf. [13]). If L^h is regular, (6.1) and (6.2) provide the same result.

The evaluation of $\overline{\lambda}_r$ is considerably simplified by the following theorem, which is motivated by remarks on strong alignment, the flow being aligned with the grid, in [2] (see also [3:§10.1.1]).

Theorem 6.1. *Given an arbitrary linear residual operator with constant coefficients and a restriction operator of the form (4.3). Then the multigrid convergence factor for the shortest wave in the x- or y-direction can not be better than the convergence factor for this wave of the relaxation scheme used.*

Proof. Consider the shortest wave in the y-direction ($\theta_y = \pi$, $\hat{T}_y = -1$). In physical space this wave is described by

$$v^h_{k_1,2k_2} = -v^h_{k_1,2k_2+1} = v^h_{k_1,2k_2+2}, \quad k_1 = 0,1,\ldots,N_1-1, \quad k_2 = 0,1,\ldots,\tfrac{1}{2}N_2-1. \tag{6.3}$$

The restriction operator I^{2h}_h causes this wave to vanish on the coarser grid

$$v^{2h} = I^{2h}_h v^h = 0 \quad (\theta_y = \pi). \tag{6.4}$$

For an arbitrary linear residual operator L^h with constant coefficients we have

$$I^{2h}_h L^h v^h = L^h I^{2h}_h v^h, \tag{6.5}$$

which implies that the coarse-grid residual vanishes. As a result, the coarse-grid correction operator K (4.1) has no effect: $K = I$. The convergence factor of the multigrid scheme for this specific wave is therefore completely determined by the relaxation scheme used. The same is true for the shortest wave in the x-direction. □

This theorem has a rather unpleasant consequence for the application of any multigrid method to the differential equations under study, as pointed out by Brandt [2: §2.1, §3.3]. The rule of thumb in designing relaxation schemes is that they must remove the high-frequency part of the error. The coarse-grid correction operator will take care of the low frequencies. However, we run into problems for a purely convective equation like the fourth component of (2.4). Because convection is a locally one-dimensional phenomenon, a *differential* operator for pure convection will not depend on the structure of the flow field perpendicular to a streamline. Any good discretisation of this operator will have the same property. Suppose that a streamline is aligned with one of the grid-lines, say the x-direction. According to the rule of thumb, the relaxation scheme must remove the high frequencies, also the ones perpendicular to the streamline. But the residual corresponding to the convection operator will not depend on waves in this direction, so they can not be removed directly by relaxation. They actually *must* remain unaffected. However, for problems with boundaries, the boundary data will require the error-components in the perpendicular direction to vanish. This information can be communicated to the discrete solution only by a relaxation scheme acting along the x-direction (for those waves that have a high frequency in the y-direction and can not be represented on coarser grids). This will require $O(N_1)$ single-grid iterations for any relaxation scheme that uses only local data. Thus, a grid-independent convergence factor can never be obtained.

We will now determine lower limits of $\overline{\lambda}_r$ for the relaxation schemes of the previous section. Only the fourth component of (2.4) is considered, with $u > 0$ and $v = 0$, i.e.,

$$L^h = \frac{u}{h}(1 - T_x^{-1}), \tag{6.6}$$

which describes one-dimensional flow along the x-axis. We assume $\theta_y = \pi$, and derive $\rho(\hat{S})$ for the various relaxation schemes.

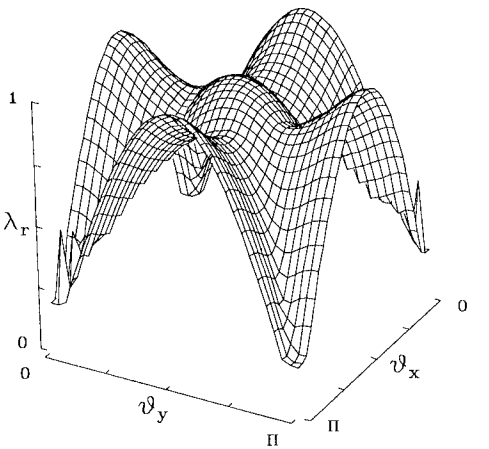

Fig. 1. *Multigrid convergence factor $\lambda_r(\theta_x, \theta_y)$ for one sweep of Red-Black relaxation followed by a coarse-grid correction. Parameters used are $u = v = 0.5$, $c = 1$, and $\beta = 1$. The instability occurs at $\lambda_r(0, \frac{1}{2}\pi) = \lambda_r(\frac{1}{2}\pi, 0) = 1.074$. The local maximum in the center of the figure $\lambda_r(\frac{1}{2}\pi, \frac{1}{2}\pi) = 1$. The figure is periodic modulo π.*

For Point-Jacobi with $0 < \beta \leq 1$, we obtain an eigenvalue λ for which

$$|\lambda|^2 = 1 - 2\beta(1-\beta)(1-\cos\theta_x). \tag{6.7}$$

This implies $\overline{\lambda}_r \geq 1 - 2\pi^2\beta(1-\beta)N_1^{-2} = 1 - O(h^2)$. For the Multi-Stage scheme, we find $\overline{\lambda}_r \geq 1 - O(h^2)$ in the same way.

The operator $\hat{S}^{RB}$ for Red-Black relaxation has two double eigenvalues

$$\lambda_\pm = 1 - \beta + \tfrac{1}{2}\beta\hat{T}_x^{-2}\left[\beta \pm \sqrt{\beta^2 + 4\hat{T}_x^2(1-\beta)}\right]. \tag{6.8a}$$

For $\beta = 1$ this results in

$$\lambda_- = 0, \quad \lambda_+ = \hat{T}_x^{-2}, \tag{6.8b}$$

implying $\overline{\lambda}_r \geq 1$ for all θ_x. For $0 < \beta < 1$ and for the long waves ($\theta_x \ll 1$) we find

$$|\lambda_-| = 1 - O(\theta_x^2), \quad |\lambda_+| = (1-\beta)^2)[1 + O(\theta_x^2)]. \tag{6.9}$$

Thus, $\overline{\lambda}_r \geq 1 - O(h^2)$. Red-Black is therefore not a suitable relaxation scheme if grid-independent convergence is desired. The situation for Red-Black is actually worse. As a single-grid scheme, RB is stable for $0 < \beta \leq 1$. Figure 1 shows that it becomes unstable in combination with the CGC operator for $\beta = 1$, just as in the one-dimensional case [13].

Block-Jacobi relaxation for the simplified residual (6.6) has two double eigenvalues

$$\lambda_1 = 1 - \beta, \quad \lambda_2 = 1 - \beta(1 - \hat{T}_x^{-2}). \tag{6.10a}$$

For $\beta = 1$ we have the same result as in (6.8b). Otherwise

$$|\lambda_1| = |1 - \beta|, \quad |\lambda_2| = [1 - 2\beta(1-\beta)(1 - \cos 2\theta_x)]^{\frac{1}{2}}. \tag{6.10b}$$

For the long waves $|\lambda_2| \simeq 1 - 2\beta(1-\beta)\theta_x^2$, implying $\overline{\lambda}_r \geq 1 - O(h^2)$. Again we have a useless relaxation scheme.

It is clear that relaxation schemes that use only local data can never provide a good multigrid convergence factor with the restriction and prolongation operator considered here.

Gauss-Seidel relaxation, which is a global scheme, may be expected to give better results, as indicated by the numerical experiments mentioned in the introduction. Indeed, GS is a natural scheme for purely convective equations, if the sweep direction coincides with the flow direction. If this is not true, then GS fails. To illustrate this, consider the fourth equations of the system (2.4), with $u \geq 0$ and $v \geq 0$, but not $u = v = 0$. The corresponding discrete residual operator is

$$\hat{L}^h = \frac{u}{h}(1 - \hat{T}_x^{-1}) + \frac{v}{h}(1 - \hat{T}_y^{-1}). \tag{6.11}$$

Then, for $\beta = 1$,

$$\begin{aligned} \hat{G}^{GS1} &= 0, & \hat{G}^{GS2} &= \frac{u\hat{T}_x^{-1} + v\hat{T}_y^{-1}}{u + v}, \\ \hat{G}^{GS3} &= \frac{v\hat{T}_y^{-1}}{u(1 - \hat{T}_x^{-1}) + v}, & \hat{G}^{GS4} &= \frac{u\hat{T}_x^{-1}}{u + v(1 - \hat{T}_y^{-1})}. \end{aligned} \tag{6.12}$$

GS1 follows the flow and is an exact solver. For the other 3 schemes, we obtain an estimated multigrid convergence factor $\overline{\lambda}_r \geq 1$ by setting either $u = 0$ and $\hat{T}_x = -1$, or $v = 0$ and $\hat{T}_y = -1$. The same is true for $0 < \beta < 1$. Consequently, GS is not an appropriate relaxation scheme for arbitrary flows.

A better performance might be expected for Symmetric Gauss-Seidel, given the experimental results mentioned in the introduction. For the residual (6.11) and $\beta = 1$ we have $\hat{G}^{GS2}\hat{G}^{GS1} = 0$, but the other combination $\hat{G}^{GS4}\hat{G}^{GS3}$ results in $\overline{\lambda}_r = 1$, e.g., for $\hat{T}_x = 1$ and $v \to 0$, given $\hat{T}_y = -1$. This can be improved by underrelaxation, using $\beta = \frac{1}{2}$. Still better results are obtained by the following form of underrelaxation:

$$\begin{aligned} &\textit{north-east } (\nearrow) \quad \hat{G}^{GS1} = 1 - \left[\hat{L}^h - A^-(1 + \hat{T}_x) - B^-(1 + \hat{T}_y)\right]^{-1} \hat{L}^h, \\ &\textit{south-west } (\swarrow) \quad \hat{G}^{GS2} = 1 - \left[\hat{L}^h + A^+(1 + \hat{T}_x^{-1}) + B^+(1 + \hat{T}_y^{-1})\right]^{-1} \hat{L}^h, \\ &\textit{south-east } (\searrow) \quad \hat{G}^{GS3} = 1 - \left[\hat{L}^h - A^-(1 + \hat{T}_x) + B^+(1 + \hat{T}_y^{-1})\right]^{-1} \hat{L}^h, \\ &\textit{north-west } (\nwarrow) \quad \hat{G}^{GS4} = 1 - \left[\hat{L}^h + A^+(1 + \hat{T}_x^{-1}) - B^-(1 + \hat{T}_y)\right]^{-1} \hat{L}^h. \end{aligned} \tag{6.13}$$

These expressions are obtained by subtracting the blocks of L^h that are ignored in the relaxation matrix $\tilde{L}^h$ for GS, from the main-diagonal of the relaxation matrix. For the residual

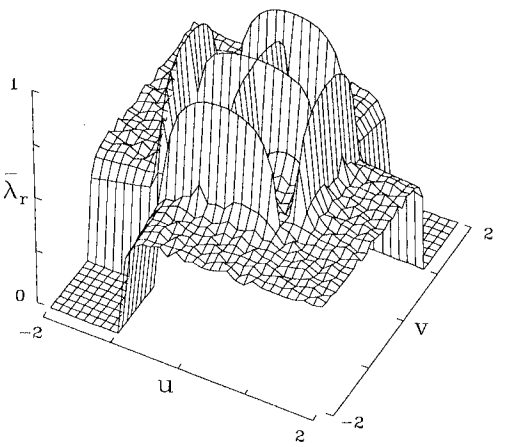

Fig. 2. *Multigrid convergence factor $\overline{\lambda}_r(u, v)$ for damped Symmetric Gauss-Seidel relaxation on a 64 × 64 grid ($c = 1$, $\nu = 1$).*

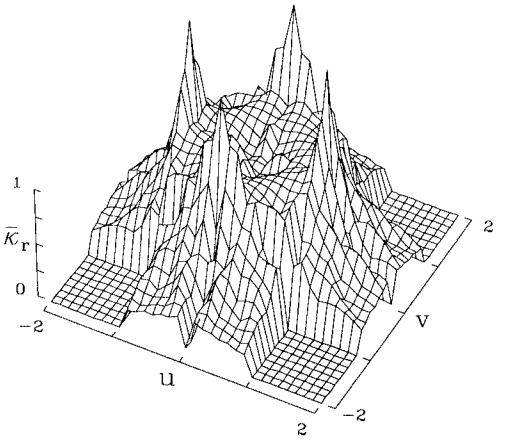

Fig. 3. *Single-grid amplification factor $\overline{\kappa}_r(u, v)$ for S^2GS, showing the instability. The values shown are obtained for $N_1 = N_2 = 64$, $c = 1$, and $\nu = 1$.*

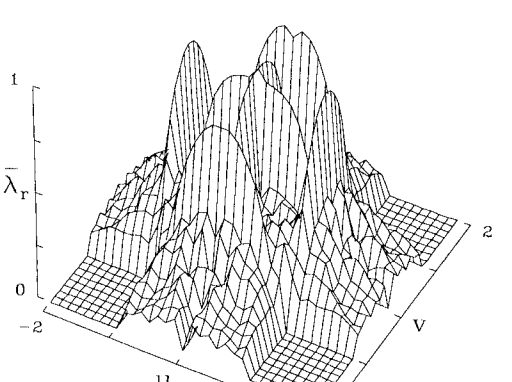

Fig. 4. *Multigrid convergence factor $\overline{\lambda}_r(u,v)$ for S^2GS, obtained for $N_1 = N_2 = 64$, $c = 1$, and $\nu = 1$. Bad convergence factors are obtained near or at the singularities of the residual.*

(6.11) it turns out that $\overline{\lambda}_r(u,v) \leq \frac{1}{2}$. Multigrid convergence factors based on $\hat{G}^{GS2}\hat{G}^{GS1}$ for the full system (2.4) are displayed in Fig. 2. Bad convergence is obtained near the singularities of the residual operator (3.8), but on the whole the convergence factors are fairly good.

There remains the combination of four sweeps denoted by S^2GS (undamped). This is an exact solver for the fourth component of the system (2.4). Also, if both the horizontal and vertical component of the velocity are supersonic, i.e., $|u| \geq c$ and $|v| \geq c$, S^2GS is exact for the full system (2.4). The convergence factor will therefore be determined by the first 3 equations of (2.4) for $|u| < c$ and/or $|v| < c$. Figure 3 shows the amplification factor for S^2GS without the use of multigrid. The quantity

$$\overline{\kappa}_r \equiv \max_{\theta_x,\theta_y} \kappa_r(\theta_x,\theta_y), \quad \kappa_r(\theta_x,\theta_y) \equiv \rho\left(\hat{L}^h \hat{S}(\hat{L}^h)^\dagger\right). \tag{6.14}$$

Surprisingly, this scheme is unstable, in contrast to SGS. The instability does not disappear for damped versions of S^2GS. Because the instability occurs for the longer waves, it can be overcome by the CGC operator, but only if $\nu = \nu_1 + \nu_2 = 1$. Applying the relaxation scheme more than once per grid per cycle causes the instability to appear in the multigrid scheme. Figure 4 shows the multigrid convergence factor for a 64×64 grid. Bad convergence factors are obtained near the singularities of the residual, namely for $u \simeq 0$ and $|v| \leq c$, for $|u| \simeq c$ and $|v| \leq c$, and for similar expressions with u and v interchanged.

Thus we find that damped SGS and S^2GS do not provide uniformly good convergence rates. However, the validity of this conclusion may be questioned, as Fourier modes are not

the proper eigenfunctions of the Gauss-Seidel relaxation operator. Therefore, some numerical experiments have been carried out.

7. Numerical experiments

The experiments are performed for flow through a straight channel, with inflow at the left side and outflow at the right. The grid is square and uniform. Upwind differencing for the full system of nonlinear Euler equations (2.1) is accomplished by van Leer's flux-vector splitting [22] or the P-variant of Osher's scheme [4,16]. For the flux-vector splitting (FVS) characteristic boundary conditions are used at the inlet and outlet, that is, the characteristic variables corresponding to x-direction are computed from the free-stream values for incoming, and from the computational domain for outgoing characteristics. From these, the boundary values and the full flux are determined. For Osher's scheme we can use overspecification. The reason for this different treatment is the fact that van Leer's FVS does not have the correct eigenvalue structure. It is not a very good approximate Riemann-solver, because it does not recognise slip-lines. Osher's scheme automatically provides the correct switching between incoming and outgoing characteristics at the inlet and outlet. The lower and upper walls are simulated by adding an extra zone with reflected state quantities (cf. [11]). The free-stream values are chosen to be

$$\rho_\infty = 1, \quad v_\infty = 0, \quad c_\infty = 1, \tag{7.1}$$

and different values of u_∞ are considered. The gas constant γ is set to 1.4. As initial conditions, we take the free-stream values and add random noise with an relative amplitude of 0.1%.

We consider both the Correction Scheme (CS) and the Full Approximation Storage (FAS) scheme, with a coarsest grid of size 1×1. The CS is used to solve the linear system arising from the application of the Switched Evolution/Relaxation (SER) method [10,23] to the residual. This is the method described in [11]. The linear system is given by

$$\left[\frac{1}{\Delta t} - \frac{dr}{dw}\right](\tilde{w} - w) = r(w) = -L(w), \tag{7.2a}$$

and the choice

$$\frac{1}{\Delta t} = \frac{1}{\varepsilon_{SER}} \max_{k_1,k_2,l} \left(\frac{|r_{k_1,k_2,l}|}{|w_{k_1,k_2,l}| + h_{k_1,k_2,l}}\right), \tag{7.2b}$$

changes the "backward Euler" scheme (7.2a) into a SER scheme. The constant ε_{SER} controls the relative change per iteration of the solution, and can usually be set to 1. The bias h_l is given by $h_1 = h_4 = 0$, $h_2 = h_3 = \rho c$, and prevents division by zero.

A nonlinear version of (7.2) has also been described in [11]. At the begin of a FAS multigrid cycle, the "time-step" (7.2b) is computed. Gauss-Seidel relaxation is carried out using a relaxation matrix that is computed locally on each grid and destroyed once used. This matrix is a modification of M_0 (5.2):

$$M_0^* = \frac{1}{\Delta t} + M_0 \quad \text{or} \quad M^*_{0\,k_1,k_2} = \frac{1}{\Delta t} - \frac{\partial r_{k_1,k_2}}{\partial w_{k_1,k_2}}. \tag{7.3}$$

After the local linear system has been solved, the residual is updated nonlinearly. A genuinely nonlinear relaxation scheme can be obtained by using (7.3) several times per point until the

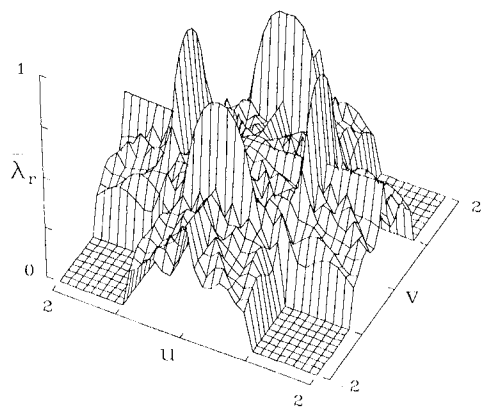

Fig. 5. *Multigrid convergence factor $\bar{\lambda}_r(u, v)$ for S^2GS on a 64×64 grid with $c = 1$ and $\nu = 1$, using van Leer's flux-vector splitting.*

local nonlinear residual vanishes. Here we will consider only one iteration per point. More iterations may be needed near shocks and sonic lines (cf.[13]).

The multigrid scheme described by Hemker and Spekreijse [4] is similar to the nonlinear one proposed in [11] but for the "time-step" (7.2b). We have included this scheme in the experiments by leaving out the $1/\Delta t$ term. In all cases, W-cycles are used, with one pre relaxation sweep ($\nu_1 = 1$, $\nu_2 = 0$).

Apart from channel flow, periodic boundaries conditions on all four sides of the domain are considered as well. In that case, a stationary solution can generally not be reached by time-accurate integration from arbitrary initial data. The artificial viscosity provided by the upwind differencing allows for convergence to a not necessarily unique numerical steady state. For the examples presented below, FVS converges to the free-stream values if global conservation of the initial date is imposed. In the FAS scheme this is carried out on the coarsest 1×1 grid; for the Correction Scheme this is done on the finest grid at the end of every multigrid cycle. Osher's scheme does not provide a unique solution for the examples considered, but the convergence factor of the residual can still be monitored.

The matrices of Eq.(3.3) can be used to predict the convergence factor for Osher's scheme, but not for van Leer's flux-vector splitting. For the latter, two-level estimates of $\bar{\lambda}_r$ now have to be computed from the matrices

$$A^{\pm} = P^{-1} \frac{\partial f^{\pm}}{\partial w'} P, \quad B^{\pm} = P^{-1} \frac{\partial g^{\pm}}{\partial w'} P. \tag{7.4}$$

If $|u| < c$ (or $|v| < c$), these matrices are different from those in Eq.(3.3). The corresponding residual operator has the same singularities as listed in Lemma 3.1 with the exception of the

one at $u = 0$ in case *(ii)*, the one at $v = 0$ in case *(iii)*, and $u = v = 0$ in case *(iv)*. FVS does not recognise the eigenvalue u (or v) going through zero. The result is a considerable amount of numerical viscosity around slip-lines, which actually helps to improve the smoothing factor because the effect of strong alignment is reduced. The multigrid convergence factors for S^2GS are shown in Fig. 5. The additional smearing at $u = 0$ or $v = 0$ removes the problem of strong alignment, but convergence is still bad near the remaining singularities.

We proceed with the numerical experiments. Convergence factors are based on the L_2-norm of the residual. First consider the single-grid instability of S^2GS. Table 1 shows the single-grid amplification factor $\bar{\kappa}_r$ for $u/c = 1.005$. The instability can be seen in the experiments with Osher's scheme, but it is not as strong as predicted. For FVS, the instability is less pronounced and does not show up in the numerical experiments. It is likely to appear on still finer grids, or for other velocities. The SER option has been not been used for the results of Table 1 ($\varepsilon_{SER} \to \infty$). Applying the SER scheme ($\varepsilon_{SER} = 1$) suppresses the instability, although convergence is not obtained. Results for the linear and nonlinear relaxation scheme, the latter with only one linear iteration per cell, are practically identical for this simple test problem.

Next we study the effect of the singularity *(iii)* of Lemma 3.1 for $v = 0$ and $0 \ll |u| \ll c$, a case of strong alignment. Only Osher's scheme is affected. FVS is not singular for the given velocities. Table 2 shows the results of the numerical experiments, using damped SGS relaxation. Convergence factors with the CS and FAS approach are practically identical, with or without the SER scheme.

Another singularity is the one at $u = c$ and $v = 0$. Here Osher's scheme and FVS have practically the same convergence factors, around 0.90. The results are again almost identical for the linear and nonlinear multigrid scheme, without or with the SER option. However, there is one exception. For Osher's scheme and channel flow, the FAS scheme without the SER option produced negative densities, causing the computer program to stop. Including the SER option removed this problem. The Correction Scheme converged normally. The divergence of the FAS scheme is caused by the coarsest grid (1×1), where the relaxation matrix becomes singular. The SER option suppresses this. The Correction Scheme does not recognise negative densities or energies during the multigrid cycle, and can therefore handle fairly large changes in the solution, as long as the final corrections to the state quantities remain reasonable.

Finally, consider the singularity at $u = v = 0$. The differential equation does not have a unique steady state in this case. Van Leer's FVS still provides a unique numerical solution because of the additional numerical viscosity. Table 3 shows convergence results on a 128×128 grid. The computer program stopped in several instances because of negative densities or strong divergence. No problems were encountered with the SER scheme.

The numerical experiments confirm the failure of damped SGS near the singularities of the residual operator. Similar results are found for S^2GS. In practical applications, the singularities, such as a shock or sonic line, will occur only an a small subset of the computational domain, so the overall convergence rate will be fairly good. However, the singularity at $v = 0$ will still result in slow convergence if the flow is aligned with the grid over a large part of the computational domain.

$u_\infty = 1.005$	Osher			FVS		
$N_1 = N_2$	$\overline{\kappa}_r$	periodic	channel	$\overline{\kappa}_r$	periodic	channel
16	0.955	0.92	0.91	0.985	0.91	0.90
32	0.960	0.88	0.87	0.995	0.89	0.89
64	1.944	1.19	1.01	0.999	0.89	0.88
128	3.964	1.28	1.16	1.231	0.97	0.87

Table 1. *Single-grid amplification factors for S^2GS on grids of various sizes, showing the instability of the scheme. The result of the local-mode analysis is denoted by $\overline{\kappa}_r$. The other values are determined from numerical experiments on the full system of nonlinear Euler equations, for periodic boundary conditions and for channel flow. The linear and nonlinear relaxation scheme provide practically identical results for the test problem considered. The SER option has not been used.*

$u_\infty = 0.200$	Osher			FVS		
$N_1 = N_2$	$\overline{\lambda}_r$	periodic	channel	$\overline{\lambda}_r$	periodic	channel
16	0.611	0.59	0.84	0.557	0.62	0.42
32	0.857	0.85	0.90	0.571	0.69	0.49
64	0.960	0.94	0.92	0.575	0.63	0.56
128	0.990	0.93	0.92	0.577	0.63	0.58

Table 2. *Multigrid convergence factors for damped SGS. The result of the local-mode analysis is denoted by $\overline{\lambda}_r$. This table illustrates the sensitivity of Osher's scheme to the singularity at $v = 0$. Results for the CS and the FAS scheme are practically identical, without or with the use of the SER scheme.*

$u_\infty = v_\infty = 0$		Osher		FVS	
MG scheme	SER	periodic	channel	periodic	channel
FAS	no	–	–	0.67	–
CS	no	0.91	–	0.67	–
FAS	yes	0.90	0.90	0.64	0.83
CS	yes	0.90	0.90	0.66	0.73

Table 3. *Multigrid convergence factors for damped SGS on a 128×128 grid, showing the effect of the singularity at $u = v = 0$. The predicted convergence rate is $\overline{\lambda}_r = 0.990$ for Osher's scheme and $\overline{\lambda}_r = 0.581$ for van Leer's flux-vector splitting. The dashes indicate cases of divergence. The SER option is obviously required for stability.*

8. Conclusions and discussion

The one-dimensional character of convection makes a multigrid method with a restriction operator that combines four cells or points on the fine grid to one on the coarser, ineffective. Grid-independent convergence rates can only be obtained if the relaxation scheme has a good damping rate for the entire spectrum, including the long waves. Relaxation schemes that use only local data, such as Point-Jacobi, Multi-Stage schemes, Red-Black relaxation, or Block-Jacobi, are thereby disqualified. This conclusion is merely a restatement of a problem described by Brandt [2], who calls it strong alignment, the flow being aligned with the grid.

A somewhat surprising result is the failure of symmetric Gauss-Seidel (damped SGS or S^2GS) relaxation, a global scheme. Earlier numerical experiments (§1) indicate grid-independent convergence factors already for undamped SGS. Furthermore, as a single-grid scheme, S^2GS is exact for a purely convective equation, and also for the full system that

represents the Euler equations, if both the horizontal and vertical velocity-component are supersonic. Therefore, one would expect S^2GS to overcome the problem of strong alignment. However, local-mode analysis shows that there are still waves that give rise to bad convergence factors near the singularities of the residual operator, both for damped SGS and S^2GS. This is confirmed by the numerical experiments on the nonlinear Euler equations described in §7, where the nonlinear upwind differencing is accomplished by Osher's scheme or van Leer's flux-vector splitting.

For practical purposes, damped SGS can still be useful, depending on the kind of singularities in the flow field. Even S^2GS can be used, although its instability as a single-grid scheme will not make it robust. The singularity at the sonic line will usually be confined to a small subset of the computational domain, so that the overall convergence factor will be fairly good. The singularity at $v \simeq 0$ (or $u \simeq 0$) will cause problems if the flow is aligned with the grid over a large part of the domain. Such a situation is bound to occur in channel flow. Indeed, Koren [8] observes slow convergence in precisely this setting. FVS does not suffer from this problem, at the expense of a lower spatial accuracy.

The numerical experiments show that the linear or nonlinear SER multigrid scheme proposed in [11] is more robust than its non-SER variant advertised by Hemker and Spekreijse [4]. Two of the relaxation schemes suggested in their paper, Red-Black and S^2GS, are unstable according to the analysis of §6. Red-Black is stable as a single-grid scheme, but becomes unstable when used in a multigrid code, whereas the opposite happens for S^2GS.

We will now discuss some alternatives that may lead to a uniformly good convergence rate. The main ideas can be found elsewhere, in various contexts [2:§3.3, 3:§10.5].

First, artificial viscosity can be added to remove the one-dimensional character of the residual operator for pure convection. This approach is recommended by Brandt [2]. It is expected that a fairly large amount is required, causing a degradation of the spatial accuracy. The latter may be avoided by Brandt's *double discretisation*. It should be noted that upwind schemes have a built-in amount of artificial viscosity, which here turns out to be insufficient for good convergence rates. More viscosity is added implicitly by van Leer's flux-vector splitting [22], as this scheme is not a very good approximate Riemann solver, but this still does not suffice to obtain uniformly good convergence rates.

Secondly, one could consider more powerful global relaxation schemes. Several options can be considered, such as Line-Jacobi, Line-Gauss-Seidel, zebra relaxation, Incomplete LU decomposition, or its line-variant. Some of these schemes have been studied for single-grid relaxation in [23]. It may be possible to design a scheme that provides a good grid-independent convergence factor at $O(N)$ cost even without multigrid ($N = N_1 N_2$ being the total number of cells or points). In [14] it is shown that damped Alternating Direction Line-Jacobi has a multigrid convergence factor $\overline{\lambda}_r(u, v) \leq 0.526$. For most values of u and v, we have $\overline{\lambda}(u, v) \simeq \frac{1}{2}$. The damping is obtained in the same way as in (6.13). The relaxation matrix is obtained by taking the main diagonal of the linearised residual operator and 2 off-diagonals in one direction. The 2 other off-diagonals are then subtracted from the main diagonal, thus leaving a tridiagonal system. Finally, a SER "time-step" must be added to the main diagonal. Here a diagonal element is understood to be a 4×4 block.

As a third alternative, a different type of coarsening can be considered that reflects the one-dimensional character of convection. Instead of 4 cells, or points, we can combine 2, thereby doubling the number of grid-levels. The direction of coarsening can be alternated when going to progressively coarser grids. The last option remains to be explored. Hopefully,

grid-independent convergence rates can be obtained without global relaxation schemes in this setting. Conceptually, it should not be necessary to use these global schemes, because the coarser grids must take care of global errors. As a first result we mention that damped Line-Jacobi and semi-coarsening result in an two-level multigrid convergence factor $\overline{\lambda}_r = \frac{1}{2}$ for the linearised Euler equations with constant coefficients. The line relaxation must be carried out in one direction and the coarsening, of 2 cells at the time, in the other direction.

The effects of nonlinear singularities, such as shocks, have not been considered in this paper. They may give rise to additional complications, just as in [13]. At this point, however, is appears to be difficult enough to find a good scheme for the linear case.

References

[1] W. K. Anderson, *Implicit Multigrid Algorithms for the Three-Dimensional Flux Split Euler Equations*, Ph. D. Thesis (1986), Mississippi State University.

[2] A. Brandt, *Guide to Multigrid Development*, Lecture Notes in Mathematics 960 (1981), pp. 220-312.

[3] W. Hackbusch, *Multi-Grid Methods and Applications*, Springer Series in Computational Mathematics 4 (1985), Springer Verlag, Berlin/Heidelberg.

[4] P. W. Hemker and S. P. Spekreijse, *Multiple grid and Osher's scheme for the efficient solution of the steady Euler equations*, Appl. Num. Math. 2 (1986), pp. 475-493.

[5] P. W. Hemker, *Defect correction and higher order schemes for the multigrid solution of the steady Euler equations*, Lecture Notes in Mathematics 1228 (1986), pp. 149-165.

[6] A. Jameson, *Solution of the Euler equations for two dimensional transonic flow by a multigrid method*, Appl. Math. Comp. 13 (1983), pp. 327-355.

[7] D. C. Jespersen, *Design and Implementation of a Multigrid Code for the Euler Equations*, Appl. Math. Comp. 13 (1983), pp. 357-374.

[8] B. Koren, *Euler flow solutions for a transonic windtunnel section*, CWI Report NM-R8601 (1986).

[9] B. Koren, *Evaluation of second order schemes and defect correction for the multigrid computation of airfoil flows with the steady Euler equations*, CWI Report NM-R8616 (1986).

[10] W. A. Mulder and B. van Leer, *Experiments with Implicit Upwind Methods for the Euler Equations*, J. Comp. Phys. 59 (1985), pp. 232-246.

[11] W. A. Mulder, *Multigrid Relaxation for the Euler Equations*, J. Comp. Phys. 60 (1985), pp. 235-252.

[12] W. A. Mulder, *Computation of the Quasi-Steady Gas Flow in a Spiral Galaxy by Means of a Multigrid Method*, Astron. Astrophys. 156 (1986), pp. 354-380.

[13] W. A. Mulder, *Multigrid for the one-dimensional inviscid Burgers' equation*, (1986), submitted to SIAM J. Sci. Stat. Comput.

[14] W. A. Mulder, *A note on the use of Symmetric Line Gauss-Seidel for the upwind differenced Euler equations*, Manuscript CLaSSiC-87-20 (1987).

[15] R. H. Ni, *A multiple grid scheme for solving the Euler equations*, AIAA J. 20 (1982), pp. 1565-1571.

[16] S. Osher and F. Solomon, *Upwind difference schemes for hyperbolic systems of conservation laws*, Math. Comp. 38 (1982), pp. 339-374.

[17] W. Schröder and D. Hänel, *A comparison of several MG-methods for the solution of the time dependent Navier-Stokes equations*, Lecture Notes in Mathematics 1228 (1986), pp. 272-284.

[18] G. Shaw and P. Wesseling, *A multigrid method for the compressible Navier-Stokes equations*, Report 86-12 (1986), Delft University of Technology.

[19] J. Steger and R. Warming, *Flux Vector Splitting of the Inviscid Gas Dynamics Equations with Applications to Finite-Difference Methods*, J. Comp. Phys. 40 (1981), pp. 263-293.

[20] B. van Leer, *Towards the Ultimate Conservative Difference Scheme. IV. A New Approach to Numerical Convection*, J. Comp. Phys. 23 (1977), pp. 276-299.

[21] B. van Leer, *Towards the Ultimate Conservative Difference Scheme. V. A Second-Order Sequel to Godunov's Method*, J. Comp. Phys. 32 (1979), pp. 101-136.

[22] B. van Leer, *Flux-vector splitting for the Euler equations*, Lecture Notes in Physics 170 (1982), pp. 507-512.

[23] B. van Leer and W. A. Mulder, *Relaxation Methods for Hyperbolic Conservation Laws*, in *Numerical Methods for the Euler Equations of Fluid Dynamics*, eds. F. Angrand, A. Dervieux, J. A. Desideri, and R. Glowinski, SIAM, Philadelphia (1985), pp. 312-333.